

Using Segmentation in CT Metal Artifact Reduction

Seemeen Karimi and Pamela Cosman

Department of Electrical and Computer Engineering
University of California, San Diego
La Jolla, CA, USA

Christoph Wald

Department of Radiology
Lahey Clinic
Burlington, MA, USA

Harry Martz

Lawrence Livermore National Laboratories
Livermore, CA, USA

Abstract—Metal artifact reduction methods in computed tomography replace the projection data passing through metals with an estimate of the true data. Inaccurate estimation leads to the generation of secondary artifacts. Data estimates can be improved by the use of prior knowledge of the projection data. In this paper, a method has been created to generate a prior image. The method uses computer vision techniques to segment regions of the initially reconstructed image and then discriminates between regions that are likely to be artifacts and anatomical structures. Results on test images show that metal artifacts are reduced and that few secondary artifacts are present, even in the case of multiple metal objects.

Keywords—metal artifact; computed tomography; mathematical morphology; sinogram in-painting

I. INTRODUCTION

Metal artifacts in computed tomography (CT) make images difficult for radiologists to read or computer methods to analyze by obscuring anatomical structures and implants in the images. Despite the existence of the problem for many years, and recent progress, there is no robust and widely accepted solution, and it continues to be a challenging problem.

CT number is a function of material linear attenuation coefficient. The CT number ranges of metal artifacts and anatomical regions overlap, as do gradient ranges. The separation of artifact from tissue is therefore not a trivial task. Metal artifact reduction (MAR) algorithms operate in Radon space, also known as sinograms and projections, so that uncontaminated Radon samples can be used to create the final image. In this work, we improve upon a class of MAR algorithms based on sinogram in-painting. We use computer vision to segment regions contaminated by metal artifacts from anatomical structures in the initially reconstructed image, henceforth called the original image. The affected regions are replaced with values from surrounding regions. Thus, a “prior” image is built, which guides sinogram sample estimation.

II. BACKGROUND

A. Causes of Artifacts

Metal artifacts are caused by beam hardening (the preferential attenuation of low energy photons in a poly-energetic X-ray beam), photon scatter, data sampling errors,

partial volume effects and photon starvation. Beam hardening and scatter are responsible for the bulk of the artifact. These are low-frequency artifacts, which appear as bright and dark shadows around the metal, obscuring the anatomy. The other causes create high frequency artifacts which usually can be removed by filtering in Radon or image space.

B. Current approaches

There are three classes of metal artifact reduction methods: sinogram in-painting [1-7], iterative reconstruction [8-10], and energy decomposition [11-13]. Iterative reconstruction requires accurate modeling of the X-ray generation and attenuation processes, which is difficult to accomplish. Another drawback is that iterative methods are slow because they require repeated reconstructions. Energy decomposition methods take into account the energy dependent attenuation of different materials. As a result, they can compensate for artifacts from beam hardening. However, two or more X-ray spectra are required for energy decomposition. While iterative reconstruction and energy decomposition are theoretically sound, sinogram in-painting is the most practical approach because it can be done quickly, and with one energy spectrum. Its most serious challenge is accurate data estimation.

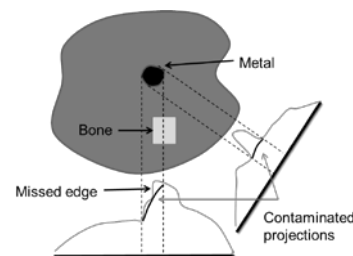


Figure 1. Direct interpolation results in missed edges.

In sinogram in-painting methods, metal traces are identified in the projections. In some methods [1-6], metal objects are located in the original image by thresholding, and the traces are located by calculation. In other methods [7], the metal traces are located directly in projections. Early work [1,2] interpolated the projection data on either side of the traces. This direct interpolation (DI) misses edges of real structures as shown in Fig. 1. Edges missed in projections result in secondary artifacts in images, which may be as severe as the metal artifacts. It was proposed that edges be recorded from the original image [3].

The edge information can be reprojected, and subtracted from the original projections. The interpolation is done in these difference projections, and the metal artifact error thus obtained is subtracted from the original projections to give the final corrected projections. However, a method for recording edge information in projections was not defined, but is critical in the performance of a MAR algorithm. Existing methods to generate a prior image that contains edge information rely on intensity thresholding [4-6]. There is much room for improvement and for the use of computer vision, in particular, in the generation of a prior image.

III. METHOD

Our method to build a prior image operates on the original image. We make two observations about metal artifacts: the artifacts are adjacent to metal pieces, and the amplitude of the artifacts decreases as the distance from the metal increases. Based on the first observation, local maxima and minima adjacent to the metal voxels are interpreted as artifacts. They are removed by replacing the voxel values with surrounding voxel values. Based on the second observation, when a local maximum contains both artifact and bone, a discriminant curve classifies voxels as artifact or bone. We restore the bone voxels to the image. Our approach, implemented in MATLAB, has the following steps. Fig. 2 shows the outputs of some steps.

A. Contouring the outer boundary

We create a closed contour along the outer boundary of the scanned anatomy, shown by the broken line in Fig. 2(a). The contour is assigned a low value of tissue (-50 HU). A contour prevents dark artifacts, if present, from blending into the surrounding air. If dark artifacts blended into the surrounding air (as shown in the rectangle), they would not be interpreted as local minima. The contour must be at least two voxels thick to prevent the later steps from removing it. If there are multiple disconnected objects in the image, and hence multiple contours, we keep only the largest one.

B. Segmentation of metal

Metal voxels are segmented by region growing. Seeds for region growing are voxels above 7000 HU. Neighboring voxels are successively added to the region if they are above 3000 HU. Teeth, which have the highest CT intensities for human tissue, are usually less than 3000 HU. Labels are generated for each connected metal region.

C. Removal of local maxima and minima

The removal of maxima and minima is performed using closing-by-reconstruction (CBR) followed by opening-by-reconstruction (OBR) [14]. CBR eliminates dark regions smaller than the size determined by the structuring element. We used a 40-voxel diameter disk as a structuring element. Next, OBR is performed to remove bright regions. CBR and OBR respectively replace voxel values in the closed or opened regions with values derived from voxels surrounding these regions. Other regions are left alone. However, the OBR and CBR operations will also remove anatomical structures, unless the anatomical structures are larger than the structuring

element. Fig. 2(b) shows the result of OBR and CBR, where anatomical structures have been eliminated along with artifacts. We restore the anatomical structures to the prior by using the following steps to discriminate between anatomy and artifacts.

D. Recovery of non-adjacent anatomical structures

The OBR and CBR processed image is subtracted from the original image. In this difference image (Fig 2c), small intensity differences, attributed to noise or artifact, are eliminated by thresholding. We used a threshold of 20 HU, which was about three times the image noise. Next, the positive and negative differences are considered separately. Region growing is performed on the negative differences. Regions of connected voxels are created that are negative with respect to the original image. Similarly, region-growing is performed on the positive differences to create connected voxel regions that are positive with respect to the original image. If the labeled regions are not adjacent to a metal label, they are interpreted as anatomical structures, and the voxel values of the original image are restored in those regions. Fig. 2(d) shows the recovery of labeled regions that are not adjacent to the metals.

E. Recovery of adjacent anatomical structures

If a region of positive artifact grows into bone, voxels containing bone would be included in the labeled region and incorrectly removed. We exploit the observation that artifact amplitude drops as a function of distance from metal. In the positive labeled regions that remain after the recovery of non-adjacent labels, voxel values of the original image are plotted against the distance transform values. The distance transform value at a voxel is the distance from that voxel to the closest metal-labeled voxel in the image. Fig. 3 shows an example plot. The artifacts generate a cluster in the plot. To find the cluster, a set of Laplacian curves is generated with different parameters. For each curve, the number of voxels under that curve is normalized by the area under the curve. The normalized number of voxels drops beyond the curve that includes the cluster. This curve is taken as the best separation of anatomy from artifact (Fig 3). Voxels above the curve are recovered because they are more influenced by anatomy than artifact. We perform this discrimination only for labeled regions that are large compared to metal, where we define large as having more than 20 times the area of the metal. We assume that these large labels must have grown into bone.

F. Correction of errors from OBR and CBR

OBR and CBR replace regions of voxels with single values. If left, the prior image would be "patchy", and the final image would have the appearance of patchy texture. To avoid this, voxel values between the limits of -50 and 200 HU are replaced with the mode value of the original image. This range includes most soft tissue, but the exact limits are not critical. Soft tissue variations will be removed. However, the soft tissue variations do not contribute to secondary artifacts, and it is better to replace them, to avoid patchiness from CBR and OBR.

The segmented metal voxels are restored to the prior image, because each metal piece is a real structure, not artifacts. This completes the generation of the prior image, shown in Fig 2(e).

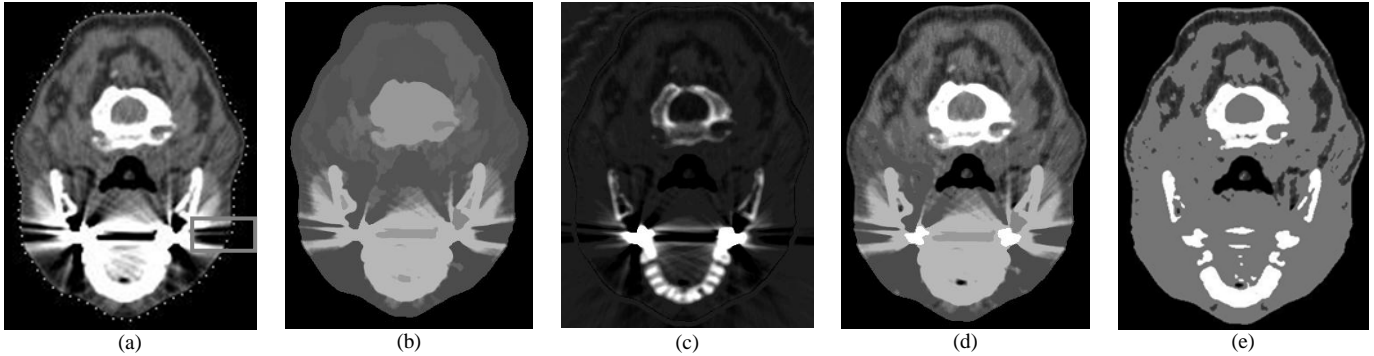


Figure 2. Stages in the generation of a prior image of a CT head scan. The contour is shown in (a), the image after CBR and OBR in (b), the difference image (a – b) in (c), the recovery of non-adjacent labels in (d) and the final prior image is in (e).

G. Replacement of Sinogram Data

The prior (Fig. 2e) is then reprojected, and the metal trace is found in the reprojections. The method described in [3] is followed for data replacement. We differ from [3] in that we fit a second order spline to five samples on both sides of the trace instead of linear interpolation. Linear interpolation of two samples should not be relied upon because sampling errors and noise will result in poor estimates of data. Alternatively, other methods of data replacement may be used, such as [6].

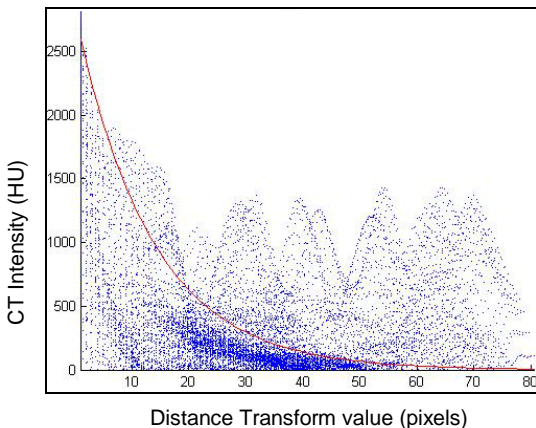


Figure 3. Graph showing the relationship between the image intensity and the distance transform for the image in Fig. 2.

IV. RESULTS

Our method was tested on axial head CT scans. Fig. 4 shows four sets of images with metal artifacts produced from metal coils in cerebral aneurysms (columns 1 and 4), from a deep brain stimulator (column 2), and from dental fillings (column 3). The original images and images corrected by our MAR algorithm are shown. For comparison, the DI [1] results are also shown. A spline is used in the DI, instead of linear interpolation as it is usually defined. The comparison shows that the prior is what determines the improvement. Artifacts are removed by our algorithm even for multiple metal pieces, and large metal pieces, which represent improvements over methods in existing literature. In contrast, DI produces secondary artifacts comparable to the original metal artifacts.

V. DISCUSSION

A. Comparison with other methods

Our algorithm preserves anatomical structures in the prior, which is why secondary artifacts are reduced. DI results in the loss of edges, so estimated data are inconsistent with the rest of the sinogram and generate secondary artifacts (Fig. 4).

Our algorithm is capable of correctly detecting artifacts of large amplitude because we use observations about the nature of metal artifacts, and more sophisticated computer vision techniques to isolate them. A previous MAR method to generate a prior was to classify each voxel of the original image into one of five tissue classes and assign it the value of the closest class [5]. The reprojection of the prior directly produced data estimates to replace the contaminated ones. However, this method fails when image voxels in the original image have artifacts of large enough amplitude that they are misclassified as air or bone. Another MAR algorithm is one that estimates the data by interpolating the ratio of the original projections to the reprojections of the prior [6]. The prior is generated by thresholding the image into air, soft tissue or bone. With misclassification, the ratio produces large errors. So, the method requires a first-pass MAR (DI is used) to provide an image with smaller amplitude artifacts so that thresholding is more likely to create a good prior. However, we demonstrate in Fig. 4 that DI may create an image that is worse than the original image. Results from [5] and [6] are not shown.

B. Future work

We have had a small set of images for testing. A larger data set should be tested involving different anatomical regions. Segmentation techniques should be investigated as alternatives to OBR and CBR. Segmentation and discrimination should be extended to three dimensions.

We used a two-dimensional relationship between distance from metal and artifact amplitude. A higher dimensional space may be investigated, including the gradient and other predictors of artifacts, for better discrimination of artifacts from bone.

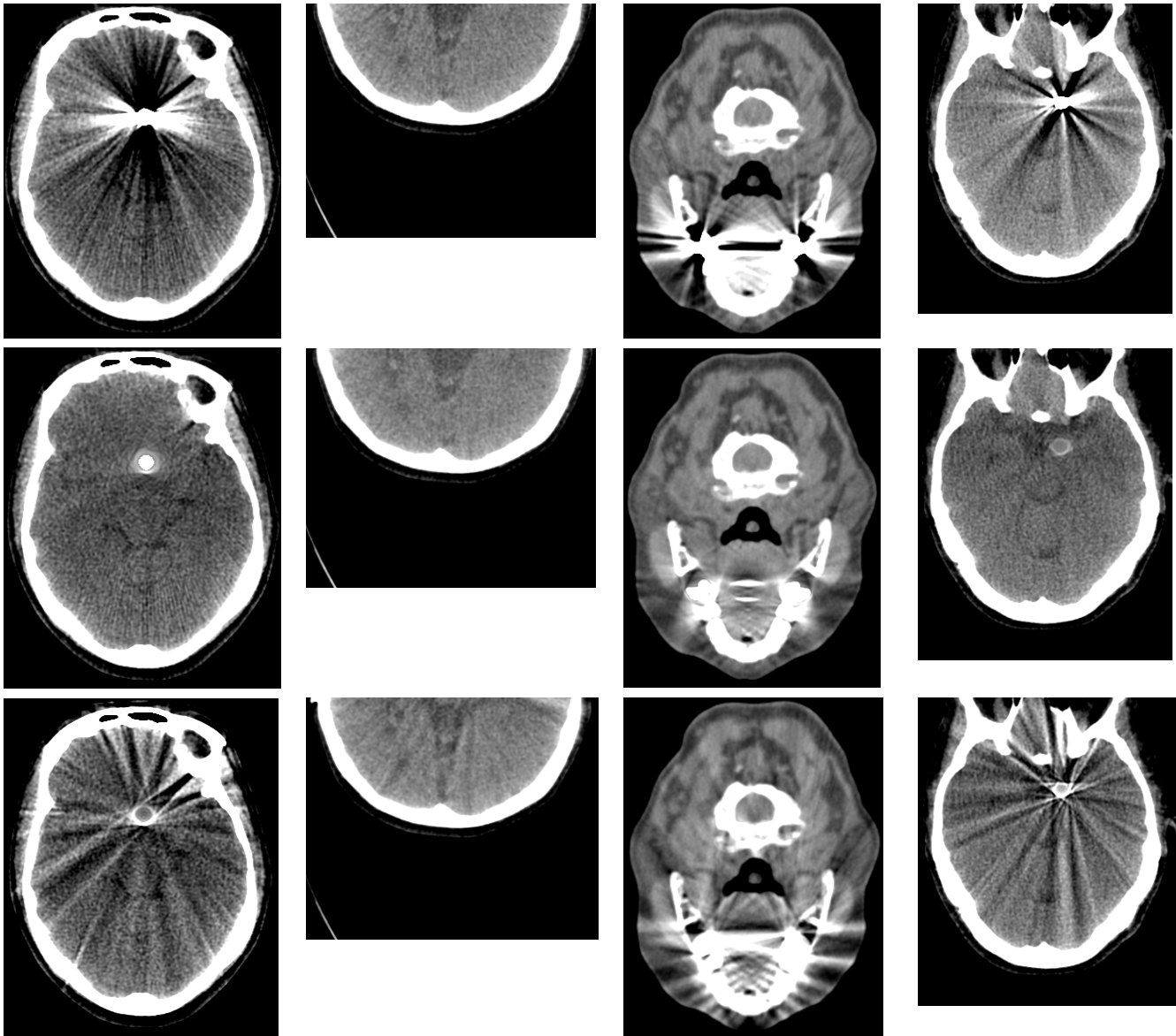


Figure 4. Four sets of images are shown in columns. For each set, the original image is on top, our MAR method image is in the middle, and the DI image is on the bottom. In all cases, the new method is an improvement over the original image and over DI.

ACKNOWLEDGMENT

The authors thank Dr. Xiaoqian Jiang. This work was sponsored by Lawrence Livermore National Laboratories.

REFERENCES

- [1] G. Glover and N. Pelc, "An algorithm for reduction of metal clip artifacts in CT reconstructions," *Med. Phys.* 8 (6), 1981.
- [2] W. Kalender R. Hebel and J. Ebersberger, "Reduction of CT artifacts caused by metallic implants," *Radiology*, vol 164 (2), 1987.
- [3] R. Naidu et al., "Method of and system for reducing metal artifacts in images generated by X-ray scanning devices," US Patent 6,721,387, 2004.
- [4] H. Li, L. Yu, X. Liu, J. Fletcher, and C. McCollough, "Metal artifact suppression from reformatted projections in multislice helical CT using dual front active contours," *Med Phys.* vol. 37 (10), 2010.
- [5] M. Bal and L. Spies, "Metal artifact reduction in CT using tissue-class modeling and adaptive filtering," *Med. Phys.*, vol. 33 (8), 2006.
- [6] E. Meyer. R. Raupach, M. Lell, B. Schmidt, M. Kachelries, "Normalized metal artifact reduction in CT," *Med. Phys.* vol. 37 (10) 2010.
- [7] W. Veldkamp et al., "Development and Validation of segmentation and interpolation for metal artifact suppression," *Med Phys.*, vol 37 (2), 2010.
- [8] X. Zhang and J. Wang, "Metal artifact reduction in X-ray computed tomography by constrained optimization," *Med. Phys.* 38 (2) Feb. 2011.
- [9] B. deMan et al., "Reduction of metal streak artifacts in x-ray CT using a transmission MAP algorithm," *IEEE, TMI* vol 47, 2000.
- [10] G. Wang, T. Frei and M. Vannier, "Fast Iterative Algorithm for Metal artifact reduction in Xray CT," *Acad Radiol.* 7 (8), August 2000
- [11] J. Sablayrolles, "CT Spectral Imaging," "AFIM 2010," <http://www.afiim.com/wp-content/uploads/2010/03/jlsablayrolles.pdf>
- [12] Bamberg et al., "Metal artifact reduction by dual energy CT using monoenergetic extrapolation," *Eur Radiol.*, 10, 2010.
- [13] Alvarez and Macovski, "Energy-selective reconstructions in X-ray computerised tomography," *Phys. Med. Biol.*, 21 (5), 1976.
- [14] R. Gonzalez, R. Woods and S. Eddins, "Morphological Image Proc.," Ch. 10, *Digital Image Proc. using MATLAB*, 2nd Ed.

